ARTICLES
https://doi.org/10.1038/s41561-018-0073-0
nature geoscience

Discrepancy between simulated and observed ethane and propane levels explained by underestimated fossil emissions

Stig B. Dalsøren[1,11*], Gunnar Myhre[1], Øivind Hodnebrog[1], Cathrine Lund Myhre[2], Andreas Stohl[2], Ignacio Pisso[2], Stefan Schwietzke[3,4], Lena Höglund-Isaksson[5], Detlev Helmig[6], Stefan Reimann[7], Stéphane Sauvage[8], Norbert Schmidbauer[2], Katie A. Read[9], Lucy J. Carpenter[9], Alastair C. Lewis[9], Shalini Punjabi[9] and Markus Wallasch[10]

Ethane and propane are the most abundant non-methane hydrocarbons in the atmosphere. However, their emissions, atmospheric distribution, and trends in their atmospheric concentrations are insufficiently understood. Atmospheric model simulations using standard community emission inventories do not reproduce available measurements in the Northern Hemisphere. Here, we show that observations of pre-industrial and present-day ethane and propane can be reproduced in simulations with a detailed atmospheric chemistry transport model, provided that natural geologic emissions are taken into account and anthropogenic fossil fuel emissions are assumed to be two to three times higher than is indicated in current inventories. Accounting for these enhanced ethane and propane emissions results in simulated surface ozone concentrations that are 5–13% higher than previously assumed in some polluted regions in Asia. The improved correspondence with observed ethane and propane in model simulations with greater emissions suggests that the level of fossil (geologic + fossil fuel) methane emissions in current inventories may need re-evaluation.

Direct emissions at the surface are the only sources of ethane and propane to the atmosphere[1,2], and several studies suggest that they are underestimated in global inventories[1,3–7]. A major source of uncertainty is that these inventories first calculate total non-methane hydrocarbon (NMHC) emissions and then disaggregate them into individual species (ethane, propane and so on) based on limited amounts of data[8–11]. Over the past decade the inventories do not fully account for an abrupt increase in the exploitation of unconventional natural gas in the United States[3,4] and therefore probably underestimate present-day emissions[3,4,12–23]. Recent atmospheric model simulations that apply current global emission inventories tend to underestimate observed ethane and propane concentrations in wintertime in the Northern Hemisphere[3–5,7,12,24–29].

Anthropogenic fossil fuel (conventional and unconventional) emissions are at present the largest emission source of ethane and propane in most global inventories. Fugitive emission is the main fossil fuel NMHC source and includes venting and flaring, evaporative losses and equipment leaks, but not fuel combustion. Changes in these particular emissions are regarded as the main cause of observed ethane trends[3,4,26,30–34]. Recent studies[9,35] calculated fugitive fossil fuel emissions from oil, natural gas and coal systems for ethane based on a joint inventory and atmospheric box-model approach, and the emission data set[9] used therein was recently updated with new data[36]. Another recent study[10] used a detailed inventory approach to identify cold venting of associated petroleum gas also considering methane, propane and butane as significant emission sources that are potentially underestimated in existing emission inventories. These new studies combine field measurements and country-specific information from published sources along with observed flaring of associated gas from satellite images. In combination these take into account that the emission factors from the venting and flaring of associated gas released during extraction vary considerably across different oil, coal and gas fields around the world. Such considerations have not been made in most community emission data sets, which apply emission factors reported by countries to the United Nations Framework Convention on Climate Change, or from measurements representative for North America for those countries that are not reporting. Deficiencies in fugitive fossil fuel emission estimates in community emission data sets were also recently found for black carbon at high latitudes[37] and SO_2 at low latitudes[38] (the Middle East). Natural geologic emissions are another suggested fossil hydrocarbon source that is missing in inventories[39,40], receiving little attention in previous model studies. Major geologic sources include seepage from onshore and submarine petroleum basins, volcanoes and degassing from geothermal manifestations (see Methods). Based on the few available estimates[39,40], geologic emissions may have been the largest pre-industrial source of ethane to the atmosphere (Fig. 1a).

Another cause of poor model performance could be inaccurate representation of atmospheric sinks. Oxidation by hydroxyl (OH)

[1]CICERO, Oslo, Norway. [2]NILU, Kjeller, Norway. [3]CIRES, University of Colorado, Boulder, CO, USA. [4]NOAA Earth System Research Laboratory, Global Monitoring Division, Boulder, CO, USA. [5]International Institute for Applied Systems Analysis, Laxenburg, Austria. [6]Institute of Arctic and Alpine Research, University of Colorado, Boulder, CO, USA. [7]Empa, Laboratory for Air Pollution/Environmental Technology, Swiss Federal Laboratories for Materials Science and Technology, Dübendorf, Switzerland. [8]IMT Lille Douai, SAGE, Université de Lille, Lille, France. [9]Wolfson Atmospheric Chemistry Laboratories, Department of Chemistry, University of York, York, UK. [10]Umweltbundesamt, Messnetzzentrale Langen, Langen, Germany. [11]Present address: Institute of Marine Research, His, Norway. *e-mail: stig.dalsoeren@hi.no

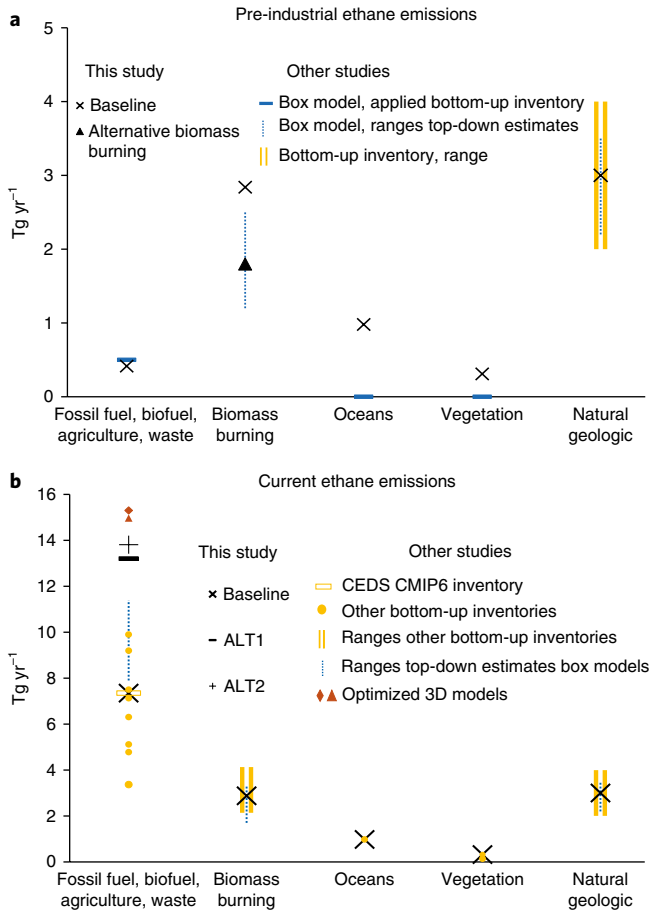

Fig. 1 | Global total sectoral ethane emissions in this study and other studies. a, Global total ethane emissions in pre-industrial simulations in this study (black symbols, see Methods section for details of alternative biomass burning emissions) compared with emissions in other studies. Box model data (blue symbols) are from ref. [39]. Bottom-up inventory data (yellow symbols) from ref. [40]. **b**, Global total ethane emissions in the year 2011 baseline and alternative (ALT1, ALT2) simulations in this study (black symbols) compared to emissions in other studies. The inventories and estimates cover the year 2000 and onwards. The closest year to our simulation year 2011 is chosen for inventories not covering that year. Bottom-up inventories (yellow symbols and bars): Fossil fuel, biofuel, agriculture, waste: CEDS CMIP6 (ref. [47] used in baseline in this study), HTAPv2, Edgar 3.2 FT, RETRO, POET, CMIP5 (average of MACCITY, ACCMIP, RCP2.6, RCP4.5, RCP6, RCP8.5) (as reported and referenced in ECCAD database: http://eccad.aeris-data.fr/), ARCTAS (ref. [7]), EDGAR4.3.2 (ref. [11]) and new inventory in ref. [56]. Biomass burning: GFEDv4 (baseline this study), GICC,ACCMIP, POET, GFASv1.2, MACCITY, RETRO, RCP2.6, RCP4.5, RCP8.5 (as reported and referenced in ECCAD database) and FINN (refs [3,4]). Oceans: RETRO (baseline this study, see Methods). Vegetation: MEGAN-MACC (baseline this study, see Methods) and MEGANv2 (as reported and referenced in ECCAD database). Natural geologic: Reported by ref. [40] (median estimate used in baseline in this study). Top-down estimates from box models (dotted blue bars): Fossil fuel, biofuel, agriculture, waste: refs [31,33,39]. Biomass burning: ref. [39]. Natural geologic: ref. [39]. Optimized emissions in 3D model studies (brown symbols): refs [3,4].

in the troposphere is the main sink for ethane and propane[1,2,41]. Estimates of global mean OH levels and hemispheric ratios differ substantially between observation-based estimates and results from model ensembles[42–44]. Studies also find large intermodel differences in the atmospheric distributions of oxidants[45].

In this study we first apply the OsloCTM3 model[46] to investigate the pre-industrial atmospheric ethane budget. We compare model results from simulations with and without geologic emissions to ice-core measurements. Thereafter, we model current conditions represented by the year 2011, which is the last year available in all applied fugitive fossil fuel emission data sets. In the year 2011 baseline simulation we use the state-of-the-art global anthropogenic emission inventory from the Community Emissions Data System (CEDS) Project used in the Coupled Model Intercomparison Project Phase 6 (CMIP6)[47]. We also include natural emissions (treated as negligible in many model studies) from oceanic, biogenic (vegetation) and geologic sources (see Methods). We compare with surface ethane and propane measurements from global and regional surface networks (see Methods) with a focus on observations in the mid- to high-latitude Northern Hemisphere, where previous model studies underestimated observations. We then generate alternative gridded emissions by replacing the fugitive fossil fuel emissions in the CEDS CMIP6 inventory with new data sets that better represent fossil fuel activity and emissions[9,10,35,36] with corrections to avoid double-counting from potential overlap with natural geologic emissions (see Methods). In the resulting alternative simulations (ALT1 and ALT2, Tables 1–2) the fossil fuel emissions are factors of about two (ethane, Fig. 1b) and three (propane, Supplementary Fig. 1) higher than in the baseline simulation with very different geographical distributions (Supplementary Fig. 2). We also suggest further modifications of the ALT1 and ALT2 emissions based on studies with the Flexpart model[48]. Back-trajectories from Flexpart are used to identify source regions related to OsloCTM3 under- and overestimation of observed ethane concentrations (see Methods). Finally, we explore the uncertainty of the atmospheric sinks in a sensitivity study where we perturb the OsloCTM3 OH level within its uncertainty range (see Methods).

Pre-industrial ethane budget

Ice-core measurements[39] reveal a large (a factor of about 4) north/south interpolar ratio for ethane. Figure 2a shows that this can be reproduced by the model with a geologic source of 3 Tg yr^{-1}, constituting about 40% of the total pre-industrial ethane emissions (Fig. 1a). With geologic emissions included in the simulations the modelled abundance at Summit in Greenland agrees with observations, and the simulated interpolar ratio improves substantially relative to observations. Without geologic sources the simulated abundance at Summit is 50% too low. This is in agreement with the findings of ref. [39], where a simpler model without interactive oxidation chemistry was used.

Our baseline simulation slightly overestimates the observed Antarctic ethane concentration. Transport to high southern latitudes and biomass burning emissions have high interannual variability. However, sensitivity simulations with meteorological input data for a different year and an alternative inventory with different geographical distribution and emission totals for biomass burning emissions (see Fig. 1a and Methods) resulted in minor changes (see Supplementary Information). We therefore suggest that a small Antarctic overestimation relates to uncertainties in the magnitude and distribution of geologic and oceanic emissions in the Southern Hemisphere.

Current ethane and propane budgets

The baseline simulation for 2011 does not reproduce the observed interpolar ethane ratio well, even if geologic emissions are included (Fig. 2b). The modelled concentration at Summit in Greenland is only about 50% of measured values (Fig. 2b). Underestimations of ethane and propane concentrations at high northern latitudes, particularly during wintertime (Fig. 3, Supplementary Figs. 3–7), are similar to most other model studies[3–5,7,12,24–29] using standard emission inventories. As shown below, the likely cause is underestimated

Table 1 | Overview of the simulations performed with OsloCTM3

Year	Simulation	Simulation name	Inventories anthropogenic and natural emissions[a]	Geologic emissions	Oxidation chemistry	Meteorological year
1750	Pre-industrial	1750 Baseline	Baseline	Yes	Interactive	2011
	Pre-industrial sensitivity	1750 NOGEO	Baseline	No	Interactive	2011
		1750 MET	Baseline	Yes	Interactive	2014
		1750 BBURN	Baseline, but CMIP5 biomass burning	Yes	Interactive	2011
2011	Baseline	2011 Baseline	Baseline	Yes	Interactive	2011
	Baseline sensitivity	OH	Baseline	Yes	Interactive, OH field scaled down in reactions with ethane and propane[b]	2011
	Alternative	ALT1	ALT1	Yes	Interactive	2011
		ALT2	ALT2	Yes	Interactive	2011

[a]The baseline, ALT1 and ALT2 emission inventories are described in the above section and the Methods. [b]The scaling of OH is described in the Methods.

fossil fuel emissions in the standard community emission data set CEDS CMIP6, used in the baseline simulation. The CEDS CMIP6 emission data[47] agree with previous emission data for ethane and propane used in atmospheric climate and air pollution studies (Fig. 1b and Supplementary Fig. 1).

The ALT1 and ALT2 simulations, where the CEDS CMIP6 fugitive fossil fuel emissions are replaced with the new data sets[9,10,35,36], reproduce the interpolar ethane ratio and the observed levels in Greenland (Fig. 2b), Zeppelin Observatory at Svalbard (Fig. 3a) and most other stations (Fig. 3b, Supplementary Figs. 3–9) much more closely. This is also the case for propane (Fig. 3a,c, Supplementary Figs. 3–9), for which fossil fuel emissions play an even larger role (Supplementary Fig. 1). A substantial improvement is found throughout the Arctic (Supplementary Fig. 5, Supplementary Tables 2 and 3). ALT1 performs better than ALT2. Both have positive mean biases, tending to overestimate episodes with high concentrations. We explore these and other episodes at Zeppelin (Arctic station with frequent sampling) in a systematic way (see Methods). Figure 4 shows that the episodes with the largest underestimation of ethane at Zeppelin in the baseline simulation occur for air masses originating from Eurasia. Fossil fuels are the dominant emission source in this region for most of the year, strongly suggesting that these are underestimated in the CMIP6 inventory. From Fig. 4, it is also evident that ALT1 underestimates the fossil fuel emissions in northwestern Europe (that is, mainly emissions from the North Sea) whereas it overestimates emissions from Russia. The ALT2 simulation mainly overestimates observed ethane levels at Zeppelin (Fig. 3a). For this inventory, the fossil fuel emissions are probably overestimated both in the North Sea and Russia (Fig. 4). Overestimated emissions in ALT1 and ALT2 over Russia also seem

Table 2 | Overview of the new fugitive fossil fuel emission inventories used in the alternative year 2011 simulations

Inventory	Natural gas	Oil	Coal
ALT1 ethane	ref. [10]	ref. [10]	ref. [9] updated with data from ref. [36]
ALT1 propane	ref. [10]	ref. [10]	ref. [9] updated with data from ref. [36]
ALT2 ethane	refs [9,35] updated with data from ref. [36]	ref. [9] updated with data from ref. [36]	ref. [9] updated with data from ref. [36]
ALT2 propane	refs [9,35] updated with data from ref. [36], but using the propane to ethane ratio from ref. [10]	ref. [9] updated with data from ref. [36], but using the propane to ethane ratio from ref. [10]	ref. [9] updated with data from ref. [36], but using the propane to ethane ratio from ref. [10]

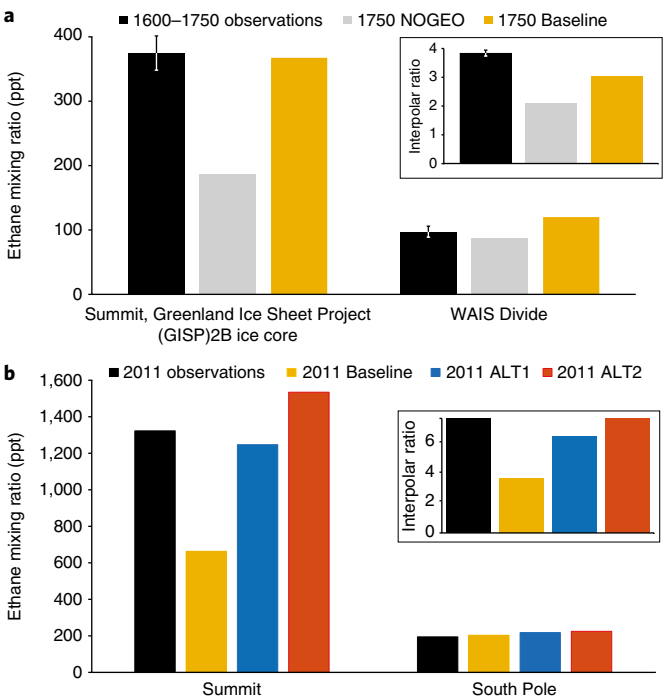

Fig. 2 | Observed and modelled annual mean ethane mixing ratios and inter-polar ratios. a, Observed (ref. [39]) and modelled (this study) pre-industrial interpolar ratio and mixing ratios at Summit, Greenland and at the West Antarctic Ice Sheet (WAIS) site. Observation error bars are the reported ±2 standard errors in ref. [39]. **b**, Observed and modelled interpolar ratio and mixing ratios in 2011. For the Antarctic, the closest station (South Pole) with data to the WAIS measurement site (no data for 2011) was used. See Table 1 for more information about the simulations.

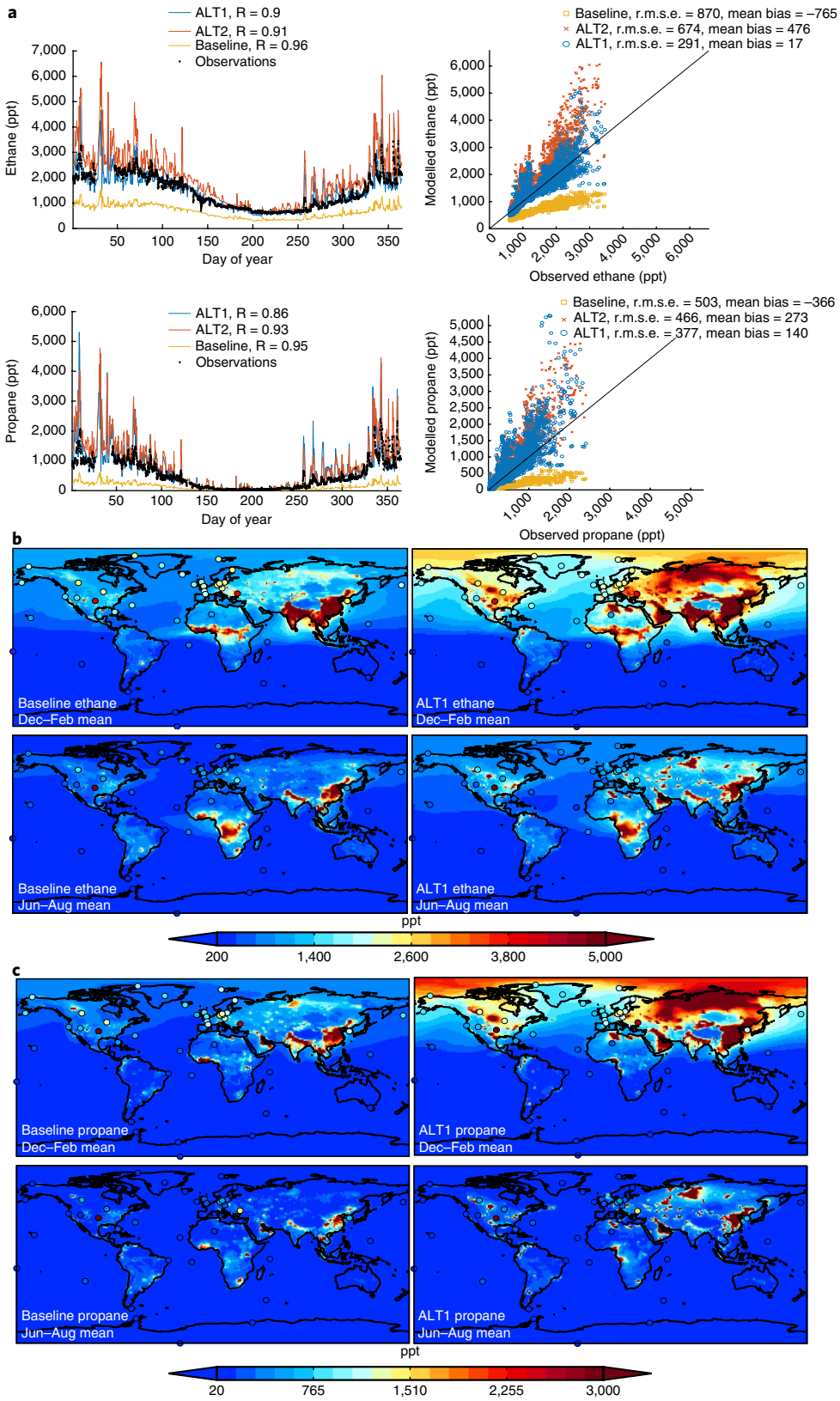

Fig. 3 | Comparison of year 2011 modelled and observed ethane and propane at surface sites. a, Comparison of modelled and observed year 2011 ethane (upper row) and propane (lower row) at the Zeppelin station. The left column shows time series and in the right column the same results are shown as scatter plots. A selection of comparisons for other sites is shown in the Supplementary Information. **b**, Comparison of modelled (background colours, simulations as indicated) and observed surface (coloured circles) of ethane for the year 2011. Model data for the lowest model layer were used. Stations with fewer than six samples within the three-month averaging period were excluded from the comparison. Mountain stations that typically sample free tropospheric air and are situated in areas where the model resolution does not resolve the terrain were also excluded. Details on the applied observation datasets are provided in the Methods section. Maps for the ALT2 simulation are shown in the Supplementary Information. **c**, Same as **b**, but for propane. r.m.s.e., root-mean-square error.

likely from the comparison with Tiksi station data (Supplementary Fig. 5, the only available station in Russia).

At mid-latitude stations in the United States and Canada, both ALT1 and ALT2 show good agreement with measurements (Supplementary Fig. 6, Supplementary Tables 2 and 3). An exception is the highly oil- and natural gas-influenced Southern Great Plains station (large underestimation, see Supplementary Fig. 6). Large emissions from several nearby oil wells might not be fully resolved in the model averaging emissions over the model grid scale. It is also a possibility that the ALT1 and ALT2 inventories underestimate the emissions from nearby unconventional gas fields (such as Woodford, Barnett[49]) and oil wells. The ALT1 and ALT2 simulations also improve agreement with measurements at non-Arctic European stations compared with the baseline (Supplementary Fig. 7, Supplementary Tables 2 and 3), especially for ethane. At most stations the ALT1 simulation is biased slightly low compared with the observations. ALT2 also performs better than the baseline, but overestimates (to varying degrees) the measurements at most European stations.

The lower-latitude Cape Verde site also shows large improvements (ALT simulations versus baseline) during wintertime (Supplementary Fig. 8) when it is influenced by air passing over the Sahara[50] from oil and gas fields in northern Africa and the Middle East. In the Southern Hemisphere, the baseline simulation reproduces observed levels and seasonal patterns well and the alternative simulations only result in minor differences (Figs. 2–3 and Supplementary Fig. 9).

The ALT1 and ALT2 anthropogenic ethane emissions (excluding biomass burning) are slightly smaller than the optimized anthropogenic emissions in other recent model studies[3,4] (Fig. 1b). The optimized emissions in other studies are based on sensitivity simulations[3,4] that find that an approximate doubling of anthropogenic emissions is needed to reproduce measurements at Jungfraujoch[4] and a few other FTIR stations in the Northern Hemisphere[3]. In our study we include natural geologic emissions and apply new detailed emission data sets for fugitive fossil fuel emissions instead of performing an upscaling of all anthropogenic emissions. Our model is also run at higher spatial and temporal resolutions and compared with a greater number of measurement sites.

Overestimated atmospheric loss (that is, too high OH levels) might lead to an underestimation of observed ethane and propane levels. However, this cannot be a major cause of the discrepancies in our baseline simulation. Scaling down tropospheric hydroxyl levels to the lower range of model and observational based estimates (see Methods) improves the agreement slightly (Supplementary Fig. 10) but much of the underestimation in the mid-high Northern Hemisphere during wintertime persists. This seasonal pattern is expected as chemical loss at high northern latitudes is inefficient during wintertime when little sunlight and low water vapour concentrations result in low OH concentrations.

We have not included atmospheric oxidation of ethane and propane by halogens in the model simulations. The reasons and the implications for uncertainty are discussed in the Supplementary Information. The inclusion of halogen chemistry would probably lead to slightly larger underestimation of ethane and propane in the baseline simulation, thereby providing support for emissions in standard community data sets being too low.

Our global total natural geologic emissions correspond with the best estimates from earlier work[40]. Reported uncertainty ranges[39,40] are shown in Fig. 1 and Supplementary Fig. 1. A recent study[51] suggests geologic methane emissions about one-third of that estimated by ref. [40]. NMHC-to-methane emission ratios from geologic sources are uncertain and probably highly spatially and temporally variable. Therefore, findings that suggest lower methane flux in the far past do not necessarily imply lower pre-industrial and present-day NMHC emissions. However, if this earlier finding[51] was applied via downscaling to estimate ethane emissions, it fits poorly with the findings of our pre-industrial simulations (Fig. 2a), unless we change the geographical distribution towards a larger fraction of emissions in the Northern Hemisphere. As noted (see Methods) the uncertainty in the geographical distribution is large.

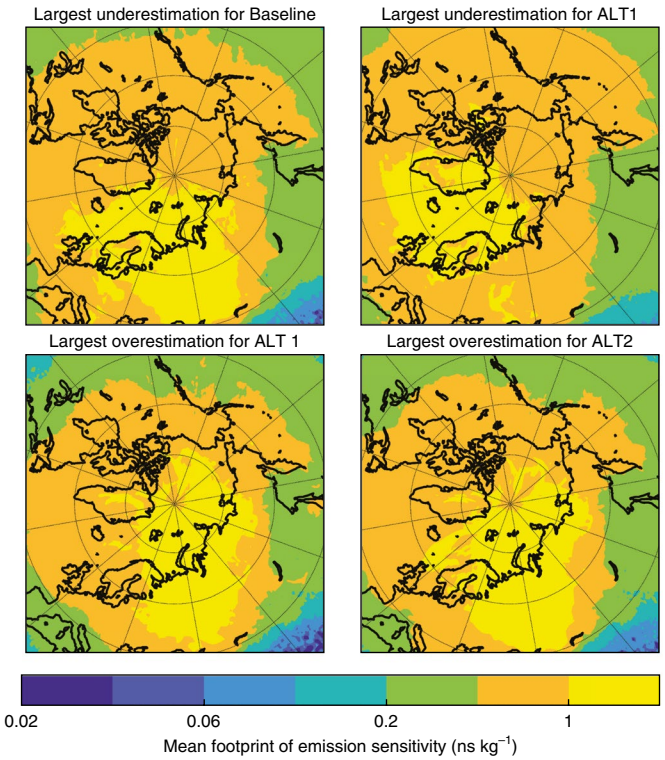

Fig. 4 | Footprints at Zeppelin. Yearly mean Flexpart footprints (see Methods for details on approach) for ethane at Zeppelin. Upper row: Episodes with the largest underestimation in the baseline (left) and ALT1 (right) simulations. Lower row: Episodes with the largest overestimation in the ALT1 (left) and ALT2 (right) simulations. The unit ns kg^{-1} is proportional to the residence time in a given volume of air.

The relative uncertainties in global total emissions in the new fugitive fossil fuel data sets (applied in the ALT1 and ALT2 inventories) are about half of those used in CEDS CMIP6 (baseline inventory) (see Supplementary Information). Another improvement is substantially reduced uncertainties in geographical emission distributions (see Methods). Based on the comparisons in the previous paragraphs the correct global total anthropogenic ethane emissions seem to be close to the levels in the ALT1 and ALT2 simulations (rectangle, triangle Supplementary Fig. 11). These levels are greater than the upper cap of the baseline uncertainty bar in Supplementary Fig. 11; that is, the baseline inventory probably underestimates emissions. The total emissions in the baseline inventory are close to the mean and median of those in eight other standard community emissions data sets, suggesting that applying these will also result in modelled ethane concentrations that are too low. For the ALT1 and ALT2 inventories, only total emissions near the lower end of the uncertainty range (Supplementary Fig. 11) reproduce the observed levels. Various model uncertainties widen the possible emission range but major ones associated with the OH sink have relatively small impacts on modelled ethane concentrations. Model uncertainties do therefore not change our conclusions regarding under- and overestimation in the different emission inventories. Using the alternative emission data sets (ALT1 or ALT2) instead of the standard community emission inventories greatly improves the comparison with observations. Owing to sparse observation coverage

in some world regions, and the uncertainty ranges of the emissions and atmospheric chemical loss of ethane and propane, we do not provide an overall performance ranking between the emission data sets ALT1 and ALT2.

Impacts on other atmospheric constituents

The higher ethane and propane in the ALT1 and ALT2 simulations compared with the baseline simulation impact the greenhouse gas methane and major surface pollutants. The impacts on tropospheric methane are moderate, leading to 0.5% (ALT1) and 0.7% (ALT2) longer methane lifetimes due to lower tropospheric OH. Modelled baseline ozone mixing ratios are compared with surface measurements in Supplementary Fig. 12 for the period June–August when ozone photochemistry is most active in the Northern Hemisphere. The model reproduces the gradients between regions with high photochemical production and cleaner background areas. At many stations the model is at, or within, a few parts per billion (ppb) (or per cent) of the measurements. In regions with high levels of surface ozone in the baseline, particularly the Middle East and eastern Asia, ozone is 5–13% (3–11 ppb) higher in spring/summer (Supplementary Fig. 13) in ALT1 and ALT2. In these regions, the ozone production is more sensitive to the amount of NMHCs as high concentrations of NO_x are present. Surface ozone differences in other regions are generally small (0–5% or 0–3 ppb). If fossil emissions of other related NMHCs are underestimated as well (for example, butane, pentane and so on), the impacts on ozone and other air pollutants will be larger. Impacts on the air pollutants NO_2, peroxyacetyl nitrate (PAN) and CO are discussed in the Supplementary Information.

Methane constitutes the largest share of hydrocarbons emitted from fossil sources, and a recent study[52] suggests underestimation of fossil methane emissions in previous estimates. Compared with previous inventories the much higher fossil fuel ethane and propane emissions in the new data sets[9,10,35,36] used in ALT1 and ALT2 in this study are mainly due to higher NMHC to methane emission ratios. The improved agreement with ice-core ethane measurements for the simulation with geologic emissions supports the idea that there is a considerable geologic methane emission source[52,53]. As for ethane and propane, geologic emissions of methane have been neglected in many model studies. In accordance with an earlier study[52], we suggest a need for more studies evaluating the reported level of fossil methane emissions in current emission inventories. Understanding the contribution from different natural and anthropogenic emission sources is a critical precursor to design efficient measures to reverse ongoing atmospheric ethane, propane and methane increasess[4,54,55].

Methods

Methods, including statements of data availability and any associated accession codes and references, are available at https://doi.org/10.1038/s41561-018-0073-0.

Received: 23 July 2017; Accepted: 29 January 2018;
Published online: 26 February 2018

References

1. Rudolph, J. The tropospheric distribution and budget of ethane. *J. Geophys. Res. Atmos.* **100**, 11369–11381 (1995).
2. Rosado-Reyes, C. M. & Francisco, J. S. Atmospheric oxidation pathways of propane and its by-products: Acetone, acetaldehyde, and propionaldehyde. *J. Geophys. Res Atmos.* **112**, D14310 (2007).
3. Franco, B. et al. Evaluating ethane and methane emissions associated with the development of oil and natural gas extraction in North America. *Environ. Res. Lett.* **11**, 044010 (2016).
4. Helmig, D. et al. Reversal of global atmospheric ethane and propane trends largely due to US oil and natural gas production. *Nat. Geosci.* **9**, 490–495 (2016).
5. Stein, O. & Rudolph, J. Modeling and interpretation of stable carbon isotope ratios of ethane in global chemical transport models. *J. Geophys. Res. Atmos.* **112**, D14308 (2007).
6. Thompson, A., Rudolph, J., Rohrer, F. & Stein, O. Concentration and stable carbon isotopic composition of ethane and benzene using a global three-dimensional isotope inclusive chemical tracer model. *J. Geophys. Res. Atmos.* **108**, 4373 (2003).
7. Emmons, L. K. et al. The POLARCAT Model Intercomparison Project (POLMIP): overview and evaluation with observations. *Atmos. Chem. Phys.* **15**, 6721–6744 (2015).
8. Li, M. et al. Mapping Asian anthropogenic emissions of non-methane volatile organic compounds to multiple chemical mechanisms. *Atmos. Chem. Phys.* **14**, 5617–5638 (2014).
9. Schwietzke, S., Griffin, W. M., Matthews, H. S. & Bruhwiler, L. M. P. Global bottom-up fossil fuel fugitive methane and ethane emissions inventory for atmospheric modeling. *ACS Sustain. Chem. Eng.* **2**, 1992–2001 (2014).
10. Höglund-Isaksson, L. Bottom-up simulations of methane and ethane emissions from global oil and gas systems 1980 to 2012. *Environ. Res. Lett.* **12**, 024007 (2017).
11. Huang, G. et al. Speciation of anthropogenic emissions of non-methane volatile organic compounds: a global gridded data set for 1970–2012. *Atmos. Chem. Phys.* **17**, 7683–7701 (2017).
12. Xiao, Y. et al. Global budget of ethane and regional constraints on U.S. sources. *J. Geophys. Res. Atmos.* **113**, D21306 (2008).
13. Zavala-Araiza, D. et al. Reconciling divergent estimates of oil and gas methane emissions. *Proc. Natl. Acad. Sci. USA* **112**, 15597–15602 (2015).
14. Karion, A. et al. Aircraft-based estimate of total methane emissions from the Barnett Shale region. *Environ. Sci. Technol.* **49**, 8124–8131 (2015).
15. Kort, E. A. et al. Four corners: the largest US methane anomaly viewed from space. *Geophys. Res. Lett.* **41**, 6898–6903 (2014).
16. Kort, E. A. et al. Fugitive emissions from the Bakken shale illustrate role of shale production in global ethane shift. *Geophys. Res. Lett.* **43**, 4617–4623 (2016).
17. Peischl, J. et al. Quantifying atmospheric methane emissions from the Haynesville, Fayetteville, and northeastern Marcellus shale gas production regions. *J. Geophys. Res. Atmos.* **120**, 2119–2139 (2015).
18. Pétron, G. et al. A new look at methane and nonmethane hydrocarbon emissions from oil and natural gas operations in the Colorado Denver-Julesburg Basin. *J. Geophys. Res. Atmos.* **119**, 6836–6852 (2014).
19. Swarthout, R. F. et al. Impact of Marcellus shale natural gas development in southwest Pennsylvania on volatile organic compound emissions and regional air quality. *Environ. Sci. Technol.* **49**, 3175–3184 (2015).
20. Vinciguerra, T. et al. Regional air quality impacts of hydraulic fracturing and shale natural gas activity: evidence from ambient VOC observations. *Atmos. Environ.* **110**, 144–150 (2015).
21. Schneising, O. et al. Remote sensing of fugitive methane emissions from oil and gas production in North American tight geologic formations. *Earth's Future* **2**, 548–558 (2014).
22. Moore, C. W., Zielinska, B., Pétron, G. & Jackson, R. B. Air impacts of increased natural gas acquisition, processing, and use: a critical review. *Environ. Sci. Technol.* **48**, 8349–8359 (2014).
23. Roest, G. & Schade, G. Quantifying alkane emissions in the Eagle Ford Shale using boundary layer enhancement. *Atmos. Chem. Phys.* **17**, 11163–11176 (2017).
24. Pozzer, A. et al. Simulating organic species with the global atmospheric chemistry general circulation model ECHAM5/MESSy1: a comparison of model results with observations. *Atmos. Chem. Phys.* **7**, 2527–2550 (2007).
25. González Abad, G. et al. Ethane, ethyne and carbon monoxide concentrations in the upper troposphere and lower stratosphere from ACE and GEOS-Chem: a comparison study. *Atmos. Chem. Phys.* **11**, 9927–9941 (2011).
26. Angelbratt, J. et al. Carbon monoxide (CO) and ethane (C_2H_6) trends from ground-based solar FTIR measurements at six European stations, comparison and sensitivity analysis with the EMEP model. *Atmos. Chem. Phys.* **11**, 9253–9269 (2011).
27. Lin, M., Holloway, T., Carmichael, G. R. & Fiore, A. M. Quantifying pollution inflow and outflow over East Asia in spring with regional and global models. *Atmos. Chem. Phys.* **10**, 4221–4239 (2010).
28. Helmig, D. et al. Climatology and atmospheric chemistry of the non-methane hydrocarbons ethane and propane over the North Atlantic. *Elementa* **3** (2015).
29. Pozzer, A. et al. Observed and simulated global distribution and budget of atmospheric C_2–C_5 alkanes. *Atmos. Chem. Phys.* **10**, 4403–4422 (2010).
30. Helmig, D. et al. Reconstruction of Northern Hemisphere 1950–2010 atmospheric non-methane hydrocarbons. *Atmos. Chem. Phys.* **14**, 1463–1483 (2014).
31. Simpson, I. J. et al. Long-term decline of global atmospheric ethane concentrations and implications for methane. *Nature* **488**, 490–494 (2012).

32. Hausmann, P., Sussmann, R. & Smale, D. Contribution of oil and natural gas production to renewed increase in atmospheric methane (2007–2014): top–down estimate from ethane and methane column observations. *Atmos. Chem. Phys.* **16**, 3227–3244 (2016).
33. Aydin, M. et al. Recent decreases in fossil-fuel emissions of ethane and methane derived from firn air. *Nature* **476**, 198–201 (2011).
34. Zeng, G. et al. Trends and variations in CO, C_2H_6, and HCN in the Southern Hemisphere point to the declining anthropogenic emissions of CO and C_2H_6. *Atmos. Chem. Phys.* **12**, 7543–7555 (2012).
35. Schwietzke, S., Griffin, W. M., Matthews, H. S. & Bruhwiler, L. M. P. Natural gas fugitive emissions rates constrained by global atmospheric methane and ethane. *Environ. Sci. Technol.* **48**, 7714–7722 (2014).
36. Sherwood, O. A., Schwietzke, S., Arling, V. A. & Etiope, G. Global inventory of gas geochemistry data from fossil fuel, microbial and biomass burning sources, version 2017. *Earth Syst. Sci. Data* **9**, 639–656 (2017).
37. Stohl, A. et al. Black carbon in the Arctic: the underestimated role of gas flaring and residential combustion emissions. *Atmos. Chem. Phys.* **13**, 8833–8855 (2013).
38. McLinden, C. A. et al. Space-based detection of missing sulfur dioxide sources of global air pollution. *Nat. Geosci.* **9**, 496–500 (2016).
39. Nicewonger, M. R., Verhulst, K. R., Aydin, M. & Saltzman, E. S. Preindustrial atmospheric ethane levels inferred from polar ice cores: a constraint on the geologic sources of atmospheric ethane and methane. *Geophys. Res. Lett.* **43**, 214–221 (2016).
40. Etiope, G. & Ciccioli, P. Earth's degassing: a missing ethane and propane source. *Science* **323**, 478–478 (2009).
41. Aikin, A. C., Herman, J. R., Maier, E. J. & McQuillan, C. J. Atmospheric chemistry of ethane and ethylene. *J. Geophys. Res. Oceans* **87**, 3105–3118 (1982).
42. Patra, P. K. et al. Observational evidence for interhemispheric hydroxyl-radical parity. *Nature* **513**, 219–223 (2014).
43. Strode, S. A. et al. Implications of carbon monoxide bias for methane lifetime and atmospheric composition in chemistry climate models. *Atmos. Chem. Phys.* **15**, 11789–11805 (2015).
44. Rigby, M. et al. Role of atmospheric oxidation in recent methane growth. *Proc. Natl Acad. Sci. USA* **114**, 5373–5377 (2017).
45. Naik, V. et al. Preindustrial to present-day changes in tropospheric hydroxyl radical and methane lifetime from the Atmospheric Chemistry and Climate Model Intercomparison Project (ACCMIP). *Atmos. Chem. Phys.* **13**, 5277–5298 (2013).
46. Søvde, O. A. et al. The chemical transport model Oslo CTM3. *Geosci. Model Dev.* **5**, 1441–1469 (2012).
47. Hoesly, R. M. et al. Historical (1750–2014) anthropogenic emissions of reactive gases and aerosols from the Community Emission Data System (CEDS). *Geosci. Model Dev.* **11**, 369–408 (2018).
48. Stohl, A., Forster, C., Frank, A., Seibert, P. & Wotawa, G. Technical note: the Lagrangian particle dispersion model FLEXPART version 6.2. *Atmos. Chem. Phys.* **5**, 2461–2474 (2005).
49. Smith, M. L. et al. Airborne ethane observations in the Barnett Shale: quantification of ethane flux and attribution of methane emissions. *Environ. Sci. Technol.* **49**, 8158–8166 (2015).
50. Carpenter, L. J. et al. Seasonal characteristics of tropical marine boundary layer air measured at the Cape Verde Atmospheric Observatory. *J. Atmos. Chem.* **67**, 87–140 (2010).
51. Petrenko, V. V. et al. Minimal geological methane emissions during the Younger Dryas–Preboreal abrupt warming event. *Nature* **548**, 443–446 (2017).
52. Schwietzke, S. et al. Upward revision of global fossil fuel methane emissions based on isotope database. *Nature* **538**, 88–91 (2016).
53. Etiope, G., Lassey, K. R., Klusman, R. W. & Boschi, E. Reappraisal of the fossil methane budget and related emission from geologic sources. *Geophys. Res. Lett.* **35**, L09307 (2008).
54. Rigby, M. et al. Renewed growth of atmospheric methane. *Geophys. Res. Lett.* **35**, L22805 (2008).
55. Dlugokencky, E. J. et al. Observational constraints on recent increases in the atmospheric CH4 burden. *Geophys. Res. Lett.* **36**, L18803 (2009).
56. Tzompa-Sosa, Z. A. et al. Revisiting global fossil fuel and biofuel emissions of ethane. *J. Geophys. Res. Atmos.* **122**, 2493–2512 (2017).

Acknowledgements

This research is funded by the Research Council of Norway through the MOCA (Methane Emissions from the Arctic Ocean to the Atmosphere: Present and Future Climate Effects) project (grant no. 225814). The Flexpart work was partially funded by the Nordic Center of Excellence eSTICC (eScience Tools for Investigating Climate Change in northern high latitudes) funded by Nordforsk (grant 57001). Furthermore, the conclusions of the paper is largely supported and strengthened by the use of globally distributed observational data and we acknowledge all data providers and the great efforts of EMEP, ACTRIS, NOAA ESRL/INSTAAR and The World Data Centre for Greenhouse Gases (WDCGG) under the WMO-GAW programme to make long-term measurements public and available. The Horizon 2020 research and innovation programme ACTRIS-2 Integrating Activities (grant agreement no. 654109) is acknowledged for the work with quality assurance and quality control of NMHC data in Europe. The VOC observations within the NOAA-INSTAAR GGGRN are supported in part by the US National Oceanic and Atmospheric Administration's Climate Program Office's AC4 Program, and quality control was supported in part by the US National Science Foundation grant no. 1108391. The GLOGOS dataset was kindly provided by CGG Geoconsulting. CGG Geoconsulting also provided us with a derived product from the Global Offshore Seepage Database (GOSD) indicating where offshore seepage occurs.

Author contributions

S.B.D., G.M. and Ø.H. designed the study with input from A.S., C.L.M. and I.P. S.B.D performed the simulations with the OsloCTM3 model, analysed the model results and performed the comparisons with measurement data. Ø.H. and G.M. provided assistance with the analysis and comparison studies. I.P performed the simulations with the Flexpart model and I.P. and A.S. analysed the output. S.Schwietzke and L.H.-I. provided the new emission datasets for fugitive fossil fuel emissions. S.B.D. developed gridded inventories for geologic emissions. C.L.M, D.H., S.R., S.S., N.S., K.A.R., L.J.C., A.C.L., S.P. and M.W. provided the observational data for ethane and propane. S.B.D. led the writing of the manuscript in close collaboration with G.M. and Ø.H. All authors contributed to the writing and review of the manuscript.

Competing interests

The authors declare no competing interests.

Additional information

Supplementary information is available for this paper at https://doi.org/10.1038/s41561-018-0073-0.

Reprints and permissions information is available at www.nature.com/reprints.

Correspondence and requests for materials should be addressed to S.B.D.

Publisher's note: Springer Nature remains neutral with regard to jurisdictional claims in published maps and institutional affiliations.

Methods

Models. *OsloCTM3.* We use the OsloCTM3 model[46] to simulate the pre-industrial (year 1750) and current (year 2011) distributions of atmospheric ethane and propane. The model is run with approximately 1.1°×1.1° (T159) horizontal resolution. To spin up the model 15 month simulations were made with coarse resolution (2.2°×2.2°) followed by 4 month simulations with 1.1°×1.1° (T159) resolution. After the spin-up a set of simulations (Table 1) were made. A coupled tropospheric and stratospheric 60-layer (surface-0.1 hPa) version is used with 100 chemical active species that affect atmospheric oxidation capacity. OsloCTM3 was described and evaluated by ref. [46] and was used in several studies related to atmospheric oxidation capacity[57].

The OsloCTM3 simulations are driven with three-hourly year 2011 meteorological forecast data from the European Centre for Medium-Range Weather Forecasts (ECMWF) Integrated Forecast System (IFS) model (see ref. [46] for details). These data are 36-hour forecasts produced with 12 hours of spin-up starting from an ERA-Interim analysis at noon on the previous day.

Flexpart. To investigate the origin of air masses observed at the Zeppelin station, we use version 9.2 of the LPDM FLEXPART (FLEXible PARTicle dispersion model)[48]. The model is driven with three-hourly operational meteorological analyses from the ECMWF with 91 vertical levels and a horizontal resolution of 1°×1°. Computational particles released from the location of the Zeppelin station are tracked 20 days back in time in FLEXPART's 'retroplume' mode. The model output consists of an emission sensitivity, the surface footprint of which is used here to identify source regions related to OsloCTM3 under- and overestimation of observed ethane concentrations.

Emissions and model simulations. *Baseline emission inventories all constituents.* For anthropogenic SO_x, NH_3, CO, NO_x and NMHC emissions, we use the CEDS Project emission inventory[47] for the years 1750 and 2011, the state-of-the-art data set currently used in CMIP6. For biomass burning, we use GFEDv4[58] year 2011 emissions and the historical biomass burning data set for CMIP6 for 1750[59]. Sulfur emissions from other sources are described in ref. [60]. Non-methane volatile organic compound (NMVOC) emissions from vegetation and oceans are neglected (set to zero) in some studies but not in this study. Biogenic emissions of CO and NMVOCs from vegetation are set to year 2010 (the last year covered by the data set) emissions from MEGAN-MACC[61] both for the pre-industrial and year 2011 simulations. For NO_x from soil and CO and NMHCs from the oceans we use the year 2000 emissions in the RETRO inventory[62]. Lightning NO_x emissions are described in ref. [46]. For natural NH_3 sources we use emissions from GEIA[63] for 1990. Methane emissions are described in ref. [57].

Geologic emissions of ethane and propane. For ethane and propane we include the geologic emissions suggested by ref. [40] in the baseline emission inventories. For both 1750 and 2011 the global total emissions are set to the medians (3 Tg yr^{-1} for ethane, 1.7 Tg yr^{-1} for propane) of the ranges (2–4 Tg yr^{-1} ethane, 1–2.4 Tg yr^{-1} propane) estimated by ref. [40]. Their study splits the emissions into six main geologic sources: mud volcanoes, gas seeps, microseepage, submarine seeps, geothermal manifestations and volcanoes. The geographical distribution of geologic emissions has not been gridded to files suitable for atmospheric modelling studies. Here we use several data sets to develop gridded inventories. The emissions from gas seeps (macroseepage) and mud volcanoes are distributed in accordance with the GLOGOS data set, which lists more than 2,000 terrestrial (onshore) seeps from 87 countries. In addition to site locations, GLOGOS provides measured or estimated (visually) fluxes of methane for a few sites and methane, ethane and propane concentrations in the gas for some more sites. However, the majority of sites lack such information and we therefore distribute the emissions evenly across the sites to obtain the global total macroseepage emissions estimates from ref. [40]. For submarine seeps we used a derived product (see Acknowledgements) from the Global Offshore Seepage Database (GOSD) indicating where offshore seepage occurs. We scale the density map from this data set to obtain the global total emissions from marine seepage in ref. [40]. We assume zero emissions from marine seepage in grid-boxes that are fully covered by sea-ice. For emissions from microseepage we use the CGG Robertson Tellus Sedimentary Basins of the World Map to distribute the emissions from ref. [40]. Microseepage, which is diffuse exhalation from soil in petroleum basins, is the largest geologic source but also the most uncertain one[40,64] in terms of magnitude and geographical distribution. We spread the emissions evenly over the world's petroleum basins, which represents the potential area for such diffusion, and we probably overestimate the geographical extent to some degree. We assume that permafrost or thick ice- and snow-layers hinder diffusion. The northward and southward extent of emissions is therefore limited to 66 °N and 60 °S to account for this in a simplified way. The emissions from volcanoes and geothermal sources are gridded using the geographical distribution for SO_2 emissions[60] for such activity. Geologic seepage (macroseepage, some microseepage and marine seepage) occur at many of the places where current oil, gas and coal extraction take place.

Baseline and alternative year 1750 pre-industrial ethane emissions and simulations. The pre-industrial baseline simulation (Table 1) includes geologic emissions of the magnitude suggested by ref. [40] and within the range found by ref. [39] (Fig. 1a). In the latter study an observed interpolar ethane asymmetry requires a certain combination of emissions from biomass burning and natural geologic sources (Fig. 1a). Pre-industrial biomass burning emissions are particularly uncertain, and the magnitude in the inventory (CEDS CMIP6 year 1750) in our baseline simulation is high compared with the range obtained by ref. [39]. We therefore perform an additional simulation using a biomass burning inventory (CMIP5 1850[65]) with lower emissions (Table 1, Fig. 1a) and different geographical distribution. Transport to high southern latitudes has interannual variability. To check the sensitivity in our results we do a simulation with meteorological input data for a different year (Table 1).

Baseline year 2011 ethane and propane emissions and simulation. Figure 1b shows global total sectoral ethane emissions used in the year 2011 baseline simulation in this study compared with emissions used in other inventories. Based on the pre-industrial simulations we include geologic emissions in our baseline simulation for current conditions (year 2011). Except for the box-model optimized inventory for 2000–2010 in ref. [39], geologic emissions were not included in any other model studies. Our applied emissions for biomass burning (GFEDv4 year 2011) are in the middle of the range compared with other inventories. The other anthropogenic emissions (the sum of fossil fuel, biofuel, agriculture and waste in Fig. 1b) in the CEDS CMIP6 data[47] applied in this study are quite close to the median of the estimates in other inventories. Owing to likely trends in anthropogenic emissions over the past few decades[3,4,31,33], different basis years partly explain the large range of the emission estimates in various inventories presented in Fig. 1b. The other reason is the large uncertainties in existing inventories due to incomplete approaches and data sets (discussed in main text and section below). Summing up all sectors in Fig. 1b our total emissions are in the upper range of other studies. This is mainly due to the inclusion of geologic emissions.

Alternative year 2011 ethane and propane emissions and simulations. We also perform simulations with alternative ethane and propane emissions from the energy sector (Table 1). In these we replace emissions from the energy sector in the CEDS CMIP6 inventory with two new data sets[9,10,35,36] for upstream (fuel production, gathering and processing) and downstream (transmission and distribution) emissions from oil, gas and coal systems. These studies account for the emission factors from venting and flaring of associated gas released during extraction varying considerably across different oil, coal and gas fields in the world much more comprehensively than other works. The studies used novel approaches to quantify and attribute methane and NMHC emissions, combining field measurements and country-specific information from published sources with observed flaring of associated gas from satellite images to arrive at country-specific emissions from flows of associated gas. Two simulations are performed with these data sets. In what we refer to as the ALT1 simulation emissions from oil and gas from ref. [10] are combined with coal emissions from ref. [9] (updated with data from ref. [36]) to obtain a complete inventory for the energy sector. In the ALT2 simulation we use oil, gas and coal emissions from refs [9,35] updated with data from ref. [36]. The data set does not include propane emissions and we use the global mean propane to ethane emission ratio from the ref. [10] data sets to obtain propane emissions for the ALT2 simulation. In ALT2 we use the low estimate for natural gas from ref. [9] as it was shown to be the most likely[35]. Table 2 provides an overview of the fugitive fossil fuel emissions in the ALT1 and ALT2 inventories. Owing to substantial geographical overlap it is likely that some emissions from geologic seepage are included[35] in fugitive fossil fuel inventories. To avoid double-counting, we subtract ethane and propane emissions from the oil, gas and coal grids. In the absence of a well-established gridded emission inventory of geologic seeps, we subtract geologic seepage ethane and propane emissions from oil, gas and coal grids in equal parts, that is, one-third each. By reducing with amounts corresponding to all emissions from geologic seepage, the resulting inventories (ALT1 and ALT2) could be regarded as lower estimates of emissions from current oil, gas and coal activity relative to ref. [10] and ref. [9].

Uncertainties in baseline and alternative anthropogenic emission inventories. The uncertainty calculations for the baseline inventory and alternative (ALT1, ALT2) inventories are discussed in the Supplementary Information in relation to Supplementary Fig. 11.

Sensitivity simulation on atmospheric sink. Oxidation by OH in the troposphere is the main sink for ethane and propane[1,2,41]. The uncertainty for the reaction rates is rather small, 15–20% at 298 K[2,66]. For OH concentrations, the uncertainty is larger. Our global averaged tropospheric OH (1.35×10^6 molecules per cm^3) in our 2011 baseline simulation is on the high side compared with other model studies[45]. The same holds for the hemispheric OH ratio (1.55) compared with model- and observation-based estimates[42,44]. The modelled global average methane lifetime, which is highly dependent on the modelled OH concentration, is also low compared with observation-based estimates[67,68]. We therefore did a sensitivity study scaling down the global mean OH concentration to 1×10^6 molecules per cm^3. The scaling was done separately for the hemispheres to also get a hemispheric ratio of 1. This is in the lower range of model- and observation-based estimates both for the

OH concentration and hemispheric ratio and was done to see to what degree lower OH concentrations in the Northern Hemisphere would improve the comparison with observations. The OH concentration was scaled down only in the chemical reactions with ethane and propane and not in reactions with other atmospheric constituents.

Measurement data. More and more high-quality measurements of NMHC have become available through coordination by the World Meteorological Organization (WMO) Global Atmospheric Watch (GAW) programme. Participating networks include ACTRIS (Aerosol, Clouds, and Trace gases Research Infrastructure, the European Research Infrastructure for the observation of Aerosol, Clouds, and Trace gases; http://www.actris.eu), EMEP (The European Monitoring and Evaluation Program) and NOAA ESRL/INSTAAR (National Oceanic & Atmospheric Administration Earth System Research Laboratory/Institute for Arctic and Alpine Research). To reveal the strengths and discrepancies in model performance and evaluate emission inventories we compare the model results with surface ethane and propane observations for the year 2011. We use data from surface sites reported to the World Data Center for Greenhouse Gases (WDCGG; http://ds.data.jma.go.jp/gmd/wdcgg/) following the NOAA/INSTAAR and WMO-GAW measurement protocols, and from EMEP complying with ACTRIS recommendations. EMEP and ACTRIS data were downloaded from EBAS (http://ebas.nilu.no) and are also accessible through the ACTRIS data portal (http://actris.nilu.no). These data follow the ACTRIS quality assurance procedures and protocols. Generally, the ACTRIS data have higher time resolution (up to 2 hours). Intercomparison exercises[69–71] have shown that data from NOAA/INSTAAR and EMEP/ACTRIS measurement sites are consistent within the data-quality objective of ±10% of the WMO-GAW programme[72,73].

A subset of data from 96 sites out of a total of 132 sites (66 for both ethane and propane) are shown in the comparisons for 2011. The observations at the given location, altitude and time were compared with output for the closest model grid box, level and time. Figure 3 shows all sites and Supplementary Fig. 4 shows the locations of the subset of sites selected for detailed comparison to model results. Criteria for selection included data-quality assurance, access to continuous timeseries with few gaps, coverage of different regions and site characteristics (for example, elevation, topography and the influence of pollution episodes) that are likely to be captured by the resolution of a global model.

A comparison between modelled and observed ozone is performed in the Supplementary Information and the applied ozone measurement data are presented there.

Code availability. We have opted not to make the computer codes associated with this paper available, because replication of our results does not require access to the computer codes.

Data availability. The ethane and propane surface measurement data used in this study are freely available. We use data reported to the World Data Center for Greenhouse Gases (WDCGG) (http://ds.data.jma.go.jp/gmd/wdcgg/). EMEP and ACTRIS data are available from EBAS (http://ebas.nilu.no), and are also accessible through the ACTRIS data portal (http://actris.nilu.no). The sites used for detailed comparison with model results are listed in Supplementary Table 1. The sites can easily be found by name or map search in the databases. The new emission datasets for fugitive fossil fuel emissions are available upon request from L.H.I. (hoglund@iiasa.ac.at) and S.S. (stefan.schwietzke@noaa.gov). The gridding used to develop geologic ethane and propane emissions suitable for atmospheric modelling studies was based on commercial datasets owned by CGG Geoconsulting. CGG Geoconsulting should be contacted and consulted for the task of gridding geologic emissions.

References

57. Dalsøren, S. B. et al. Atmospheric methane evolution the last 40 years. *Atmos. Chem. Phys.* **16**, 3099–3126 (2016).
58. van der Werf, G. R. et al. Global fire emissions and the contribution of deforestation, savanna, forest, agricultural, and peat fires (1997–2009). *Atmos. Chem. Phys.* **10**, 11707–11735 (2010).
59. van van Marle, M. J. E. et al. Historic global biomass burning emissions based on merging satellite observations with proxies and fire models (1750–2015). *Geosci. Model Dev.* **10**, 3329–3357 (2017).
60. Berglen, T., Berntsen, T., Isaksen, I. & Sundet, J. A global model of the coupled sulfur/oxidant chemistry in the troposphere: the sulfur cycle. *J. Geophys. Res. Atmos.* **109**, D19310 (2004).
61. Sindelarova, K. et al. Global dataset of biogenic VOC emissions calculated by the MEGAN model over the last 30 years. *Atmos. Chem. Phys.* **14**, 9317–9341 (2014).
62. Pulles, T. et al. *Reanalysis of the Tropospheric Chemical Composition Over the Past 40 years: A Long-term Global Modeling Study of Tropospheric Chemistry Funded Under the 5th EU Framework Programme* EU-Contract No. EVK2-CT-2002-00170 (ed. Schultz, M.) (GEIA, Retro, 2008).
63. Bouwman, A. F. et al. A global high-resolution emission inventory for ammonia. *Glob. Biogeochem. Cycles* **11**, 561–587 (1997).
64. Etiope, G. & Klusman, R. W. Microseepage in drylands: flux and implications in the global atmospheric source/sink budget of methane. *Glob. Planet. Change* **72**, 265–274 (2010).
65. Lamarque, J. F. et al. Historical (1850–2000) gridded anthropogenic and biomass burning emissions of reactive gases and aerosols: methodology and application. *Atmos. Chem. Phys.* **10**, 7017–7039 (2010).
66. Atkinson, R. Kinetics of the gas-phase reactions of OH radicals with alkanes and cycloalkanes. *Atmos. Chem. Phys.* **3**, 2233–2307 (2003).
67. Prinn, R. G. et al. Evidence for variability of atmospheric hydroxyl radicals over the past quarter century. *Geophys. Res. Lett.* **32**, L07809 (2005).
68. Prather, M. J., Holmes, C. D. & Hsu, J. Reactive greenhouse gas scenarios: systematic exploration of uncertainties and the role of atmospheric chemistry. *Geophys. Res. Lett.* **39**, L09803 (2012).
69. Rappenglück, B. et al. The first VOC intercomparison exercise within the Global Atmosphere Watch (GAW). *Atmos. Environ.* **40**, 7508–7527 (2006).
70. Hoerger, C. C. et al. ACTRIS non-methane hydrocarbon intercomparison experiment in Europe to support WMO GAW and EMEP observation networks. *Atmos. Meas. Tech.* **8**, 2715–2736 (2015).
71. Plass-Dülmer, C., Schmidbauer, N., Slemr, J., Slemr, F. & D'Souza, H. European hydrocarbon intercomparison experiment AMOHA part 4: Canister sampling of ambient air. *J. Geophys. Res. Atmos.* **111**, D04306 (2006).
72. Schultz, M. G. et al. The Global Atmosphere Watch reactive gases measurement network. *Elem. Sci. Anth.* **3**, 67 (2015).
73. Helmig, D. et al. Volatile organic compounds in the global atmosphere. *Eos* **90**, 513–514 (2009).